Synergy of Ag and AgBr in a Pressurized Flow Reactor for Selective Photocatalytic Oxidative Coupling of Methane

Chao Wang, Xiyi Li, Yifei Ren, Haimiao Jiao, Feng Ryan Wang, and Junwang Tang*

Read Online

ACCESS | Metrics & More | Article Recommendations | Supporting Information

ABSTRACT: Oxidation of methane into valuable chemicals, such as C_{2+} molecules, has been long sought after but the dilemma between high yield and high selectivity of desired products remains. Herein, methane is upgraded through the photocatalytic oxidative coupling of methane (OCM) over a ternary Ag−AgBr/TiO_2 catalyst in a pressurized flow reactor. The ethane yield of 35.4 μmol/h with a high C_{2+} selectivity of 79% has been obtained under 6 bar pressure. These are much better than most of the previous benchmark performance in photocatalytic OCM processes. These results are attributed to the synergy between Ag and AgBr, where Ag serves as an electron acceptor and promotes the charge transfer and AgBr forms a heterostructure with TiO_2 not only to facilitate charge separation but also to avoid the overoxidation process. This work thus demonstrates an efficient strategy for photocatalytic methane conversion by both the rational design of the catalyst for the high selectivity and reactor engineering for the high conversion.

KEYWORDS: *oxidative coupling of methane, pressurized flow reactor, synergy of Ag and AgBr, ethane, photocatalysis*
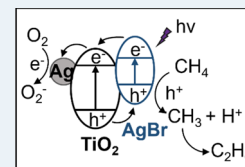
■ INTRODUCTION

Large reserves of natural gas and shale gas, especially those in remote areas, have raised incentives for the on-site and large-scale conversion of methane (CH_4) to high-value chemicals, which also avoids adverse environmental impact due to the nearly 30-time more potent greenhouse gas effect of methane than CO_2.[1,2] However, the low polarisability and high C−H bond energy (439 kJ/mol) of CH_4 make its economic conversion extremely challenging.[3] Methane conversion, including the nonoxidative coupling of methane, oxidative coupling of methane (OCM), and partial oxidation of methane, has been developed in thermocatalysis for the production of value-added products, such as C_{2+} hydrocarbons and alcohols.[4−6] However, most of the processes require strong oxidants (H_2O_2 or H_2SO_4) and/or harsh reaction conditions (e.g., high temperature and pressure).[4,7,8]

Photocatalysis uses the energy of photons instead of heat to drive thermodynamically nonspontaneous reactions, such as water splitting, carbon dioxide reduction, etc. Since photons are the main energy source, photocatalytic reactions can be conducted under very mild conditions. Methane oxidation by oxygen gas to C_1 oxygenates (e.g., CH_3OH, CH_3OOH, and HCHO) in the presence of water has been well-studied using oxide-based photocatalysts. The selectivity of products can be manipulated via the modification of different co-catalysts.[9] For instance, a high primary products (CH_3OOH and CH_3OH) yield of 25.4 μmol/h and a selectivity of 95% were achieved over TiO_2 modified by Au-CoO_x dual co-catalyst.[10] Up to now, photocatalytic methane conversion has already been achieved over TiO_2, ZnO, WO_3, etc.[11−17] However the upgrade of methane into C_2 products is still one of the most challenging pathways as it is difficult to minimize overoxidation while maintaining a high conversion rate.[18−21] Recently, CH_4 was successfully converted into C_2H_6 at a selectivity of 90% in a photochemical looping process by an Ag-HPW/TiO_2 photocatalyst.[22] However, the ethane yield (2.3 μmol/h) was very moderate, and a subsequent catalyst recovery process was required to regenerate the active silver species on TiO_2. More importantly, when O_2 was introduced into the reaction atmosphere, only overoxidation products (CO_x) were obtained.[23]

Apart from the selection of photocatalysts, the reaction system is equally important for an efficient photochemical process. Most of the reported reactors used in photocatalytic methane conversion were batch reactors.[24] However, the products in a batch reactor easily undergo overoxidation in the presence of oxidants because all products from methane conversion are more reactive than methane itself. Thus, the use of flow reactors in photocatalytic methane conversion is crucial to manipulate the mass transfer, thus minimizing the drawback of batch reactors and improving the selectivity of the less stable valuable chemicals. Our group reported the first photocatalytic OCM in a flow reaction system, an improved ethane (C_2H_6) yield of 6.8 μmol/h was achieved, but it was still quite moderate.[19] Very recently, Au-ZnO/TiO_2 was also reported for photocatalytic OCM in a flow reactor under atmospheric pressure.[25] A high C_2H_6 yield of 100 μmol/h was obtained
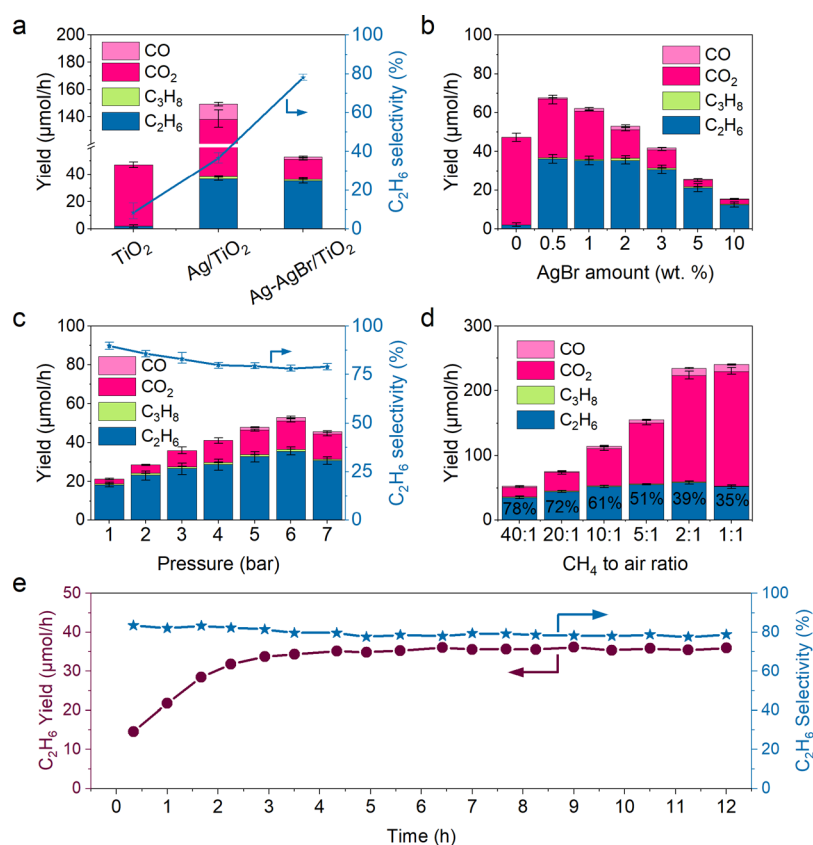
Figure 1. Photocatalytic oxidative coupling of methane: (a) products yield and C_2H_6 selectivity over TiO_2, Ag/TiO_2, and $Ag–AgBr/TiO_2$; (b) products yield over TiO_2 modified by different amounts of AgBr (based on wt % of metallic Ag); (c) products yield and C_2H_6 selectivity over $Ag–AgBr/TiO_2$ under different pressures; (d) influence of CH_4 to air ratios on the yield under 6 bar over $Ag–AgBr/TiO_2$; and (e) long-term C_2H_6 production rate and selectivity under 6 bar pressure over $Ag–AgBr/TiO_2$. Reaction conditions: flow rates of CH_4, Air, and Ar are 40, 1, and 360 mL/min, respectively, 6 bar (except c), 40 °C, 365 nm LED, and 100 mg photocatalysts. The error bar was obtained by carrying out three tests under identical reaction conditions.

without external heating, although the temperature of the catalyst reached 413 K due to Xe lamp irradiation. These results indicate it is still challenging to achieve a high yield of C_2 products at low temperatures. Moreover, the reaction pressure, as a crucial factor in gas phase reactions, has not been investigated in flow systems for photocatalytic methane conversion. Considering the high pressure of natural gas in both production sites and transportation pipelines, it is economical to convert methane in pressurized reactors.

Herein, we report the selective photocatalytic OCM in a pressurized flow reactor over an $Ag–AgBr/TiO_2$ catalyst. The ethane production rate of 35.4 μmol/h was achieved, together with an excellent C_{2+} selectivity of 79% operated at a low temperature of 40 °C. The utilization of a pressurized flow reactor likely enhanced the mass transfer of both reactants and products. Ag serves as an electron sink, while AgBr forms a heterostructure with TiO_2, which improves charge separation and migration, and more importantly avoids overoxidation. Overall, the results suggest that both the photocatalyst and the reaction system play important roles in photocatalytic methane conversion.

■ RESULTS AND DISCUSSION

Ag and AgBr were loaded on anatase TiO_2 by a two-step precipitation–photodeposition method as detailed in the Materials Synthesis (Supporting Information) and denoted $Ag–AgBr/TiO_2$. The same amount of Ag was also loaded on

TiO_2 by photodeposition as a reference and denoted Ag/TiO_2. The photocatalysts were tested in a pressurized flow reaction system (Scheme S1). The control experiment shows that the photocatalyst, CH_4, and light irradiation are all indispensable to converting methane at low temperatures (Figure S1). Then, CH_4 conversion was evaluated on TiO_2. Bare TiO_2 produces CO_2 with a selectivity of 91% at a rate of 45.1 μmol/h (Figures 1a and S2). With 2 wt % Ag deposited on TiO_2, the C_2H_6 production rate increases from 2.1 μmol/h to 36.7 μmol/h. Additionally, C_3H_8 is also produced at a rate of 1.9 μmol/h. Ag loading can facilitate the formation of C_{2+} products. However, severe overoxidation is also observed as the CO_2 production rate surges to 99.5 μmol/h, corresponding to a selectivity of 52%. When Ag and AgBr were co-loaded on TiO_2, the C_2H_6 and C_3H_8 production rates slightly reduce to 35.4 and 1.1 μmol/h, respectively, while CO_2 production is substantially suppressed. A high C_{2+} selectivity of 79% has been achieved over $Ag–AgBr/TiO_2$ in contrast to 8% over TiO_2 and 44% over Ag/TiO_2.

Following this, a series of $Ag–AgBr/TiO_2$ photocatalysts with various Ag loading amounts were synthesized to optimize the photocatalytic performance under the reaction pressure of 6 bar (Figures 1b and S2). The selectivity shifts toward C_2H_6 (70%) even with a small AgBr amount of 0.5 wt %. Increasing the amount of AgBr to 2 wt % has little effect on the yield of C_2H_6 but effectively decreases the production of CO_2. Although further increasing the AgBr amount can improve

C_{2+} selectivity to as high as 90%, a decrease in the yield of all products is observed. The results indicate that AgBr plays an important role in controlling overoxidation during methane conversion. TiO_2 decorated with 2 wt % AgBr was then chosen for further study to improve both the yield and selectivity of C_2H_6. The effect of reaction pressure on the photocatalytic OCM performance was investigated (Figures 1c and S3). The yield of C_2H_6 increases from 18.2 to 35.4 $\mu mol/h$ as the reaction pressure elevates from 1 to 6 bar. An apparent quantum efficiency under 6 bar based on methane conversion was calculated to be 3% at 365 nm. The photocatalytic performance at 7 bar stops increasing, which is possibly caused by the limited photo-induced carriers generated by the photocatalyst. The enhanced performance under elevated pressures is mainly due to the enhanced mass transfer, which increases the adsorption of CH_4 on the surface of photocatalysts. On the other hand, the selectivity of CO_2 gradually increases from 9 to 16% as pressure increases. The partial pressures of both CH_4 and O_2 in the reaction atmosphere increase as the total pressure increases. Considering the activation of O_2 is much easier than that of CH_4,[26] O_2 reduction is improved more significantly than CH_4 under higher pressures, resulting in the formation of excessive O_2^- radicals, which contributes to overoxidation. Thus, the selectivity toward C_{2+} products decreases under higher pressures. The effect of CH_4 to air ratio on the photocatalytic performance was next investigated at a total flow rate of 400 mL/min (Figures 1d and S4). When changing the ratio of CH_4/air ratio from 40:1 to 1:1, the C_2H_6 production rate first increases from 35.4 to 58.1 $\mu mol/h$ at the CH_4/air of 2:1, and finally drops to 52.1 $\mu mol/h$ when the CH_4/O_2 ratio reaches 1:1. The yield of CO_2 is greatly accelerated with the increase of O_2 proportion.

The optimized Ag−AgBr/TiO_2 photocatalyst was further tested under 6 bar pressure to examine its long-term durability (Figures 1e and S5). The yield of all products increases in the first 3 h and becomes stable afterward. It suggests that there is an in situ activation process. It is well known that AgBr is light-sensitive and can decompose into Ag and Br_2 upon exposure to irradiation.[27] The enhancement of plasmonic Ag signal in the UV−vis diffuse reflectance spectrum (DRS) of Ag−AgBr/TiO_2 after reaction for 3 h suggests that the amount of Ag in the photocatalyst increases, indicating AgBr underwent partial decomposition at this stage (Figure S6). The reduced Br 3d X-ray photoelectron spectroscopy (XPS) signal after the photocatalytic OCM reaction for 3 h and the similar intensity of the XPS peaks after running for 3 and 12 h suggest that AgBr is not fully decomposed even after the long-term irradiation (Figure S7). The main Ag species in AgBr/TiO_2 before the photocatalytic reaction are positively charged silver (Figure S8i, e.g., AgBr), with only a small amount of metallic Ag. After the reaction for 3 h, the portion of metallic Ag increases while Ag^+ decreases. This results from the fact that AgBr is partially decomposed into metallic Ag at the first 3 h of irradiation. The ratio of Ag to AgBr is calculated to be 1.34:1 based on the integrated area of the corresponding band after the catalyst is run for 3 h. Further prolonging the reaction time to 12 h results in a slight increase of Ag with an Ag to AgBr ratio of 1.57:1. The XPS results further confirm that AgBr almost remains and the chemical state of Ag in Ag−AgBr/TiO_2 is hardly changed during the photocatalytic OCM reaction from 3 to 12 h. X-ray diffraction (XRD) also confirms the partial decomposition of AgBr after 3 h and the amount of

AgBr is relatively stable in the subsequent 9 h (Figure S9), consistent with the reported.[28] Photoluminescence (PL) spectra display improved separation of charge carriers in Ag−AgBr/TiO_2 after 3 h of reaction (Figure S10). A similar luminescent property was observed in the photocatalyst after 3 and 12 h of methane conversion. Combined with the long-term photocatalytic performance, the above results reveal that AgBr is rather stable after the initial in situ activation process. Table S1 shows the performance of different reported photocatalysts for photocatalytic C_2H_6 production from methane, and it is clear that Ag−AgBr/TiO_2 shows a high C_2H_6 production rates of 34.5 $\mu mol/h$ in photocatalytic methane oxidation by air with a C_{2+} selectivity of 79% in a low reaction temperature of 40 °C.

XRD patterns of the photocatalysts display the main component of anatase (Figure 2a). Ag was not detected in
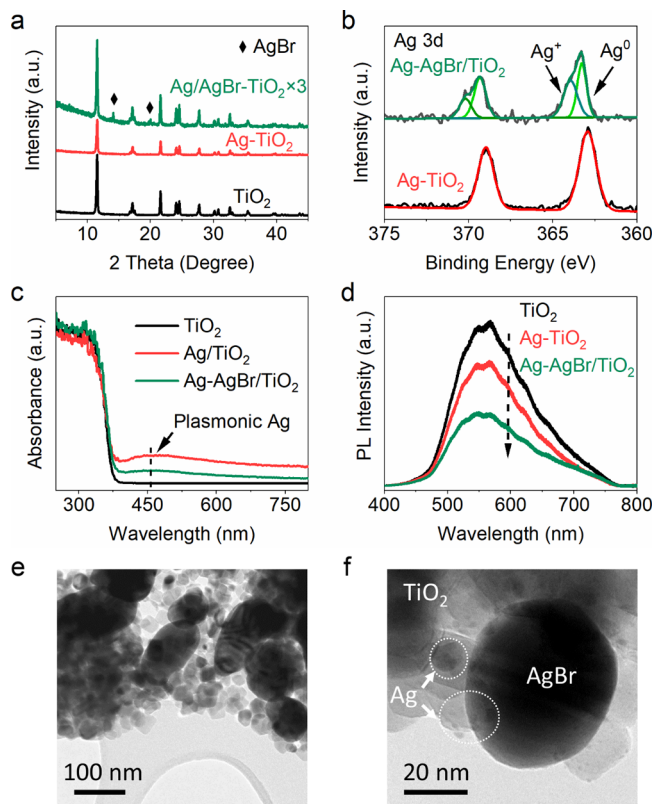
Figure 2. (a) XRD spectra of TiO_2, Ag−TiO_2, and Ag−AgBr/TiO_2; (b) Ag 3d high-resolution XPS spectra of Ag/TiO_2 and Ag−AgBr/TiO_2; (c) UV−vis DRS spectra; (d) PL spectra of TiO_2, Ag−TiO_2, and Ag−AgBr/TiO_2; and (e, f) TEM images of Ag−AgBr/TiO_2.

either Ag/TiO_2 or Ag−AgBr/TiO_2, possibly due to its small particle size and/or high dispersity.[29,30] Peaks at 14.1 and 20.0 degrees are assigned to (200) and (220) crystal planes of AgBr (PDF#06-0438), confirming the existence of AgBr on Ag−AgBr/TiO_2. Ag 3d high-resolution XPS spectra of Ag−AgBr/TiO_2 prove the presence of both metallic and positively charged Ag (Figure 2b). The peaks at 363.9 and 370.3 eV are attributed to the Ag $3d_{5/2}$ and Ag $3d_{3/2}$ of positively charged Ag ions, while those at 363.3 and 369.3 eV are ascribed to the Ag $3d_{5/2}$ and Ag $3d_{3/2}$ of metallic Ag.[31,32] The molar ratio of Ag/AgBr on the surface of TiO_2 was calculated to be 1.57:1 based on the integrated area of the related Ag $3d_{3/2}$ peak (or only 1.2 wt % of metallic Ag on the photocatalyst). Combined

with the Br 3d spectrum (Figure S7), XPS analysis reveals the co-existence of Ag and AgBr on Ag−AgBr/TiO_2. The band at 460 nm of UV−vis DRS spectra of Ag/TiO_2 and Ag−AgBr/TiO_2 is attributed to the plasmonic effect of metallic Ag (Figure 2c).[33] Absorption of AgBr is not observed in the DRS spectrum of Ag−AgBr/TiO_2, possibly due to the low loading amount. Then, the absorption spectrum of pure AgBr was measured (Figure S11), representing a visible absorption when the amount of AgBr is large enough. PL spectroscopy was used to investigate the charge separation and recombination process of the photocatalysts. TiO_2 shows the highest PL emission, implying an intense recombination process. Ag loading causes a reduction in the PL intensity, and co-modification of TiO_2 with Ag and AgBr results in the lowest PL signals. Considering the similar absorption of three catalysts in the UV region, the most efficient charge separation is achieved over Ag−AgBr/TiO_2. To further study the effect of AgBr on charge separation and migration, the open circuit photovoltage decay spectra of three catalysts were measured (Figure S12a−c). The average lifetimes of the charges in TiO_2, Ag/TiO_2, and Ag−AgBr/TiO_2 are determined to be 6.4, 12.1, and 52.9 s, respectively (Figure S12d). The eightfold increased lifetime indicates that the formation of a heterojunction between TiO_2 and AgBr significantly prolongs the charge lifetime. The longest lifetime of charge carriers is resulted from the efficient separation of electrons and holes and could improve photon efficiency in photocatalysis.

Transmission electron microscopy (TEM) images show that TiO_2 consists of nanoparticles of 20−30 nm (Figure S13a). High-resolution TEM (HRTEM) displays the (101) plane of anatase TiO_2 with an interplanar spacing of 0.346 nm (Figure S13b). Metallic Ag nanoparticles can be confirmed by the line scan of Ag/TiO_2 (Figure S14). Nanoparticles of AgBr with diameters of 100−200 nm were observed in Ag−AgBr/TiO_2 (Figure 2e). Small Ag nanoparticles of 5 nm are also found to co-exist with AgBr on TiO_2 in Ag−AgBr/TiO_2 (Figure 2f). The HRTEM (Figure S15) further verifies the existence of AgBr in Ag−AgBr/TiO_2, the interplanar distances of 0.206 and 0.290 nm are ascribed to the (220) and (200) crystal facets of AgBr, which is in accordance with the XRD analysis. In the scanning transmission electron microscopy energy-dispersive spectrometry (EDS) mapping images (Figure S16), the Ti element from TiO_2 is detected in the selected area. Ag and Br elements are consistent with large particles of AgBr. The quality of Br mapping is slightly lower than Ag. This is mainly because that AgBr is partially decomposed under the long-term irradiation of the electron beam. Overall, Ti, O, Ag, and Br are detected in Ag−AgBr/TiO_2 as observed from the EDS sum spectrum (Figure S16e).

The reduction of oxygen gas by electrons and oxidation of methane by holes are two crucial steps during photocatalytic OCM. The oxygen reduction capability of the three photocatalysts was tested via linear sweep voltammetry (LSV) in a three-electrode cell at a potential ranging from 0.4 to −1.2 V vs Ag/AgCl (Figure S17). In the absence of air, little current is generated until the applied voltage reaches −1.0 V due to hydrogen evolution. On the contrary, a negative current is generated at the onset potential of −0.4 V in the presence of air, which is attributed to the oxygen reduction reaction. Therefore, the signal obtained in the presence of air is contributed by both oxygen reduction and hydrogen evolution. To reflect the actual oxygen reduction ability of the catalysts, the difference between the LSV spectra obtained with and

without air is replotted (Figure 3a). The results show that Ag nanoparticles play a major role in oxygen reduction, as both
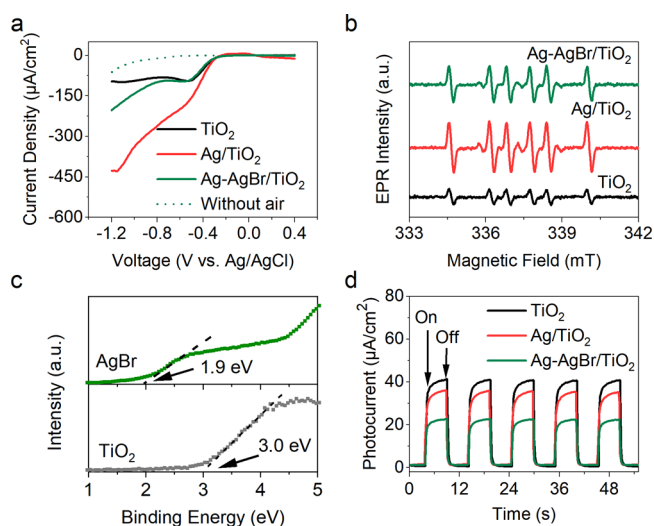

Figure 3. (a) Oxygen reduction LSV spectra of TiO_2, Ag−TiO_2, and Ag−AgBr/TiO_2 (solid line) and LSV spectrum of Ag−AgBr/TiO_2 tested in the absence of air (dotted line), (b) EPR O_2^- spectra of TiO_2, Ag−TiO_2, and Ag−AgBr/TiO_2; (c) XPS valance band spectra of TiO_2 and AgBr; and (d) transient photocurrent plots of TiO_2, Ag−TiO_2, and Ag−AgBr/TiO_2 with a bias potential of 0.25 V vs Ag/AgCl.

Ag/TiO_2 and Ag−AgBr/TiO_2 show improved current density compared with TiO_2 when the bias is more negative than −0.6 V. Ag/TiO_2 exhibits the highest current density due to the highest metallic Ag amount of 2 wt %. This is consistent with the previous report that metallic Ag could promote oxygen adsorption on TiO_2.[34] Ag acts as an electron sink and can promote charge separation by accepting electrons from the conduction band (CB) of TiO_2. Therefore, more photogenerated holes in the Ag-containing photocatalysts are available to activate methane molecules. As a result, the improved conversion rate of CH_4 is achieved after the loading of Ag. O_2 can then be reduced by electrons on the surface of Ag to produce superoxide radicals (O_2^-). To confirm this, the formation of O_2^- radicals was monitored by electron paramagnetic resonance (EPR) using 5,5-dimethyl-1-pyrroline N-oxide as the spin-trapping reagent (Figure 3b). No EPR signal is generated in dark conditions (Figure S18), suggesting that the formation of O_2^- resulted from the combination of O_2 and photoinduced electrons. Ag/TiO_2 and Ag−AgBr/TiO_2 generate a higher level of O_2^- radicals than TiO_2, which remains in the same order as the LSV oxygen reduction results when the bias is more negative than −0.6 V. The highest amount of O_2^- radicals are generated over Ag/TiO_2. O_2^- radicals clean the surface of the photocatalyst by combining with H^+ to produce H_2O. Ag serves as an electron acceptor and catalyzes O_2 reduction, which contributes to charge separation and photon efficiency, thus resulting in improved methane conversion. However, a high level of O_2^- radicals also encourage the complete mineralization of organic compounds or overoxidation to produce CO_2.[35] Thus, a large amount of CO_2 (99.5 μmol/h) was detected in the photocatalytic OCM over Ag/TiO_2. Ag−AgBr/TiO_2 shows intermediate oxygen reduction properties among three photocatalysts, which is beneficial for reducing the selectivity of CO_2 while maintaining a relatively high CH_4 conversion.

XPS valence band (VB) spectra were measured, which shows that the relative VB potentials of AgBr and TiO_2 are 1.9 and 3 eV, respectively (Figure 3c). Taking into account of the reported VB potential of anatase TiO_2 is 2.9 V vs NHE,[36] the VB potential of AgBr should be 1.8 V vs NHE. Thus, photoholes can potentially transfer from the VB of TiO_2 to AgBr in Ag−AgBr/TiO_2 upon light irradiation, resulting in a reduced oxidation potential. Thus, the overoxidation is suppressed and a high selectivity toward C_2H_6 is reasonable after the introduction of AgBr. To further evaluate the oxidation capability of the photocatalysts, the transient photocurrents of TiO_2, Ag/TiO_2, and Ag−AgBr/TiO_2 were measured in a 0.5 M $NaSO_4$ aqueous solution containing 10 vol % methanol. A bias potential of 0.25 V was applied in the test (Figures S19 and 3d). TiO_2 shows a high photocurrent density of 40 $\mu A/cm^2$, suggesting a fast electron transfer from the working electrode to the counter electrode and intensive methanol oxidation. When adding Ag to TiO_2, the photocurrent is slightly reduced somehow. It is probably because the electrons are trapped by metallic Ag, which then reduces some intermediates from methanol oxidation. When methanol is removed from the electrolyte, Ag/TiO_2 displays the highest photocurrent for water oxidation among the three catalysts (Figure S20). The lowest photocurrent is generated by Ag−AgBr/TiO_2. After photogenerated holes transfer from the VB of TiO_2 to AgBr, the oxidation potential is reduced, leading to a slow methanol oxidation process. This also mitigates the overoxidation of the produced C_{2+} to CO_2. A much higher selectivity toward C_{2+} products has thus been achieved over Ag−AgBr/TiO_2 compared with TiO_2 and Ag/TiO_2.

To provide insights into the reaction mechanism and reaction pathway, in situ diffuse reflectance infrared Fourier transform spectroscopy (DRIFTS) was performed on Ag/TiO_2 and Ag−AgBr/TiO_2 (Figure 4). The infrared (IR) signal at
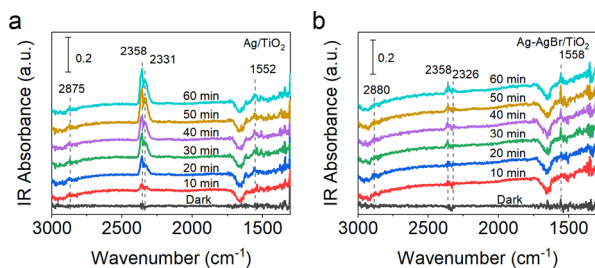

Figure 4. In situ DRIFTS spectra of Ag/TiO_2 and Ag−AgBr/TiO_2 in dark and under light irradiation in reaction atmosphere (CH_4/air = 40:1).

2875/2880 cm^{-1} under light irradiation is ascribed to the stretching vibration of C−H in $CH_3\cdot$ radicals adsorbed on the oxide surface. This band is stronger in the spectrum of Ag/TiO_2 than Ag−AgBr/TiO_2, which shows the same trend as the methane conversion performance over the two photocatalysts. The peaks at 2358 and 2331/2326 cm^{-1} are typical signals originating from CO_2 generated due to overoxidation in the photocatalytic OCM process. The CO_2 peaks over Ag/TiO_2 are much stronger than Ag−AgBr/TiO_2 and the intensity keeps increasing with prolonged irradiation time. In contrast, Ag−AgBr/TiO_2 generates a moderate amount of CO_2 under identical reaction conditions. This result is in accordance with the product selectivity of Ag/TiO_2 and Ag−AgBr/TiO_2. An additional band at 1552/1558 cm^{-1} is ascribed to the HCOO·

species, which is an important intermediate and finally results in the formation of CO_2 in the methane oxidation process. The strong band at 1558 cm^{-1} indicates that the consumption of HCOO· is slower than its formation over Ag−AgBr/TiO_2, suggesting a mild overoxidation process. However, the HCOO· species on Ag/TiO_2 can be facilely converted to CO_2, which is deduced from the low IR band intensity of HCOO· species at 1552 cm^{-1}. The IR spectra over the two photocatalysts show different features when the irradiation time reaches 70 to 120 min, as displayed in Figure S21. An increased absorption across the whole spectrum is observed over Ag/TiO_2 with the increased irradiation time. Due to the fast oxidation of methane by Ag/TiO_2, the amount of O_2 gas decreases rapidly in the reaction chamber. Therefore, photogenerated electrons could not be consumed due to the low level of oxygen and electrons start to accumulate on the CB of TiO_2, consistent with the report that the photogenerated electrons display an IR absorption from 4000 to 1500 cm^{-1}.[37] Nevertheless, this phenomenon is not observed in the IR spectra of Ag−AgBr/ TiO_2. The spectra almost overlap at the irradiation time from 70 to 120 min. This indicates that a slow oxygen consumption process and a mild methane oxidation process are achieved over Ag−AgBr/TiO_2, compared with Ag/TiO_2. This result is in accordance with the LSV oxygen reduction and EPR O_2^- trapping analysis.

To provide evidence on the universal synergy effect of Ag and AgBr on semiconductors for photocatalytic methane conversion, an Ag−AgBr/ZnO photocatalyst was synthesized by the same method, and its performance is compared with the pristine ZnO. ZnO, with a similar band structure as TiO_2, should display similar behavior as TiO_2 in photocatalytic methane conversion. The results are shown in Figure S22. When pure ZnO is applied as the photocatalyst, CH_3OH and CO_2 are generated at production rates of 6.1 and 7.5 μmol/h, respectively. It suggests that the methyl radicals formed from the reaction between methane and photoholes are mostly overoxidised into CO_2. The production of CH_3OH could probably be due to the unique surface features of ZnO, which might facilitate CH_3OH desorption. Overall, coupling of methyl radicals is not encouraged on ZnO surfaces as C_2H_6 is not detected in the products. After modification with Ag− AgBr, C_2H_6 with a high production rate of 22.8 μmol/h is detected. A trace amount of C_3H_8 (0.4 μmol/h) is also produced, which is the product of further C_2H_6 activation. CH_3OH is not detectable in the products. Most importantly, the production rate of CO_2 is reduced from 7.5 to 4.2 μmol/h after the modification of ZnO with AgBr. Combined with the methane oxidation performance of the Ag−AgBr/TiO_2 photocatalyst, direct evidence of the function of AgBr in facilitating C_2H_6 production and reducing overoxidation is obtained.

The band gaps of TiO_2 and AgBr were determined to be 3.2 and 2.5 eV, respectively, from the Kubelka−Munk conversion plots (Figure S23), consistent with the reported.[36] Combined with the XPS VB analysis (Figure 3c), the CB potentials of AgBr and TiO_2 are determined to be −0.7 and −0.3 V vs NHE, respectively. In Ag−AgBr/TiO_2, AgBr forms a type II heterojunction with TiO_2 (Scheme 1). Upon light irradiation, photoelectrons tend to transport from the CB of AgBr to TiO_2, and further to Ag, while photoholes transfer from the VB of TiO_2 to AgBr. Considering the potentials required for O_2^- formation from O_2 reduction and $\cdot CH_3$ production from CH_4 oxidation are −0.16 and 1.75 V vs NHE,[1,22,38] such a structure

Scheme 1. Photocatalytic Reaction Pathway of Ag−AgBr/TiO$_2$
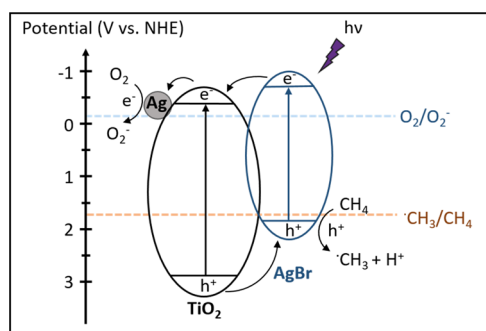
is not only beneficial for charge separation but also capable of driving the photocatalytic OCM reaction, therefore resulting in improved photon utilization efficiency and a high methane conversion. Although the enhanced charge separation is also achieved in Ag/TiO$_2$, the highly oxidative holes at the VB of TiO$_2$ and the large number of O$_2^-$ radicals formed on the metallic Ag cause severe overoxidation and significantly deteriorate the selectivity toward C$_{2+}$ products (Scheme S2 in the Supporting Information). After the introduction of AgBr, photogenerated holes at the VB of TiO$_2$ transfer to that of AgBr and then oxidize methane into methyl radicals and protons. A mild methane oxidation process is thus achieved by the less oxidative holes at the VB of AgBr. Next, the formed methyl radicals are prone to couple into C$_2$H$_6$ and are less likely to undergo overoxidation due to the relatively weak oxidation potential of photoholes in the VB of AgBr. In parallel, O$_2^-$ radicals react with protons to generate water. Some C$_2$H$_6$ molecules are activated again by photoholes to form ·C$_2$H$_5$ radicals, which couple with ·CH$_3$ radicals and form C$_3$H$_8$.

CONCLUSIONS

In summary, an efficient and selective photocatalytic OCM process has been realized with a ternary Ag−AgBr/TiO$_2$ photocatalyst in a pressurized flow reactor. The production rate of C$_2$H$_6$ achieved is as high as 35.4 μmol/h, with a C$_{2+}$ selectivity of 74−90% depending on the pressures used, together with an apparent quantum efficiency of 3% at 365 nm. These results suggest that both the reaction system and the photocatalyst play important roles in the performance of photocatalytic methane conversion as detailed by a series of characterizations. The utilization of a pressurized flow reactor enhances the mass transfer of reactants and products, contributing to the high methane conversion and selectivity toward C$_{2+}$ products. A series of electrochemical tests and EPR results proved that Ag nanoparticles serve as an electron acceptor to improve charge separation, while the reactive holes from TiO$_2$ transfer to AgBr and become less oxidative to avoid overoxidation. Therefore, both the high yield and high selectivity of C$_{2+}$ products have been obtained. The findings demonstrate a potential to realize the efficient and selective conversion of methane to C$_{2+}$ by the synergy of Ag and AgBr driven by photocatalysis.

ASSOCIATED CONTENT

Ⓢ𝕀 Supporting Information

The Supporting Information is available free of charge at https://pubs.acs.org/doi/10.1021/acscatal.2c06093.

Experimental procedures and characterization data (PDF)

AUTHOR INFORMATION

Corresponding Author

Junwang Tang − *Department of Chemical Engineering, University College London, London WC1E 7JE, U.K.; Industrial Catalysis Center, Department of Chemical Engineering, Tsinghua University, Beijing 100084, China;* ⓞ orcid.org/0000-0002-2323-5510; Email: junwang.tang@ucl.ac.uk

Authors

Chao Wang − *Department of Chemical Engineering, University College London, London WC1E 7JE, U.K.;* ⓞ orcid.org/0000-0001-5473-8244

Xiyi Li − *Department of Chemical Engineering, University College London, London WC1E 7JE, U.K.*

Yifei Ren − *Department of Chemical Engineering, University College London, London WC1E 7JE, U.K.*

Haimiao Jiao − *Department of Chemical Engineering, University College London, London WC1E 7JE, U.K.*

Feng Ryan Wang − *Department of Chemical Engineering, University College London, London WC1E 7JE, U.K.;* ⓞ orcid.org/0000-0002-2475-606X

Complete contact information is available at:
https://pubs.acs.org/10.1021/acscatal.2c06093

Author Contributions

The manuscript was written through the contributions of all authors. All authors have approved the final version of the manuscript.

Notes

The authors declare no competing financial interest.

REFERENCES

(1) Li, X.; Wang, C.; Tang, J. Methane Transformation by Photocatalysis. *Nat. Rev. Mater.* **2022**, 7, 617−632.

(2) Lashof, D. A.; Ahuja, D. R. Relative Global Warming Potentials of Greenhouse Gas Emissions. *Nature* **1990**, 344, 529−531.

(3) Meng, X.; Cui, X.; Rajan, N. P.; Yu, L.; Deng, D.; Bao, X. Direct Methane Conversion under Mild Condition by Thermo-, Electro-, or Photocatalysis. *Chem* **2019**, 5, 2296−2325.

(4) Guo, X.; Fang, G.; Li, G.; Ma, H.; Fan, H.; Yu, L.; Ma, C.; Wu, X.; Deng, D.; Wei, M.; Tan, D.; Si, R.; Zhang, S.; Li, J.; Sun, L.; Tang, Z.; Pan, X.; Bao, X. Direct, Nonoxidative Conversion of Methane to Ethylene, Aromatics, and Hydrogen. *Science* **2014**, 344, 616−619.

(5) Hutchings, G. J.; Scurrell, M. S.; Woodhouse, J. R. Oxidative Coupling of Methane Using Oxide Catalysts. *Chem. Soc. Rev.* **1989**, 18, 251−283.

(6) Woertink, J. S.; Smeets, P. J.; Groothaert, M. H.; Vance, M. A.; Sels, B. F.; Schoonheydt, R. A.; Solomon, E. I. A [Cu$_2$O]2+ Core in Cu-ZSM-5, the Active Site in the Oxidation of Methane to Methanol. *Proc. Natl. Acad. Sci. U. S. A.* **2009**, 106, 18908−18913.

(7) Periana, R. A.; Taube, D. J.; Evitt, E. R.; Löffler, D. G.; Wentrcek, P. R.; Voss, G.; Masuda, T. A Mercury-Catalyzed, High-Yield System for the Oxidation of Methane to Methanol. *Science* **1993**, *259*, 340−343.

(8) Ab Rahim, M. H.; Forde, M. M.; Jenkins, R. L.; Hammond, C.; He, Q.; Dimitratos, N.; Lopez-Sanchez, J. A.; Carley, A. F.; Taylor, S. H.; Willock, D. J.; Murphy, D. M.; Kiely, C. J.; Hutchings, G. J. Oxidation of Methane to Methanol with Hydrogen Peroxide Using Supported Gold-Palladium Alloy Nanoparticles. *Angew. Chem., Int. Ed.* **2013**, *52*, 1280−1284.

(9) Song, H.; Huang, H.; Meng, X.; Wang, Q.; Hu, H.; Wang, S.; Zhang, H.; Jewasuwan, W.; Fukata, N.; Feng, N.; Ye, J. Atomically Dispersed Nickel Anchored on a Nitrogen-Doped Carbon/TiO$_2$ Composite for Efficient and Selective Photocatalytic CH$_4$ Oxidation to Oxygenates. *Angew. Chem., Int. Ed.* **2023**, *62*, No. e2022150.

(10) Song, H.; Meng, X.; Wang, S.; Zhou, W.; Song, S.; Kako, T.; Ye, J. Selective Photo-Oxidation of Methane to Methanol with Oxygen over Dual-Cocatalyst-Modified Titanium Dioxide. *ACS Catal.* **2020**, *10*, 14318−14326.

(11) Song, H.; Meng, X.; Wang, Z.; Liu, H.; Ye, J. Solar-Energy-Mediated Methane Conversion. *Joule* **2019**, *3*, 1606−1636.

(12) Hu, D.; Ordomsky, V. V.; Khodakov, A. Y. Major Routes in the Photocatalytic Methane Conversion into Chemicals and Fuels under Mild Conditions. *Appl. Catal.. B* **2021**, *286*, No. 119913.

(13) Xie, J.; Jin, R.; Li, A.; Bi, Y.; Ruan, Q.; Deng, Y.; Zhang, Y.; Yao, S.; Sankar, G.; Ma, D.; Tang, J. Highly Selective Oxidation of Methane to Methanol at Ambient Conditions by Titanium Dioxide-Supported Iron Species. *Nat. Catal.* **2018**, *1*, 889−896.

(14) Chen, X.; Li, Y.; Pan, X.; Cortie, D.; Huang, X.; Yi, Z. Photocatalytic Oxidation of Methane over Silver Decorated Zinc Oxide Nanocatalysts. *Nat. Commun.* **2016**, *7*, 12273.

(15) Villa, K.; Murcia-López, S.; Andreu, T.; Morante, J. R. Mesoporous WO3 Photocatalyst for the Partial Oxidation of Methane to Methanol Using Electron Scavengers. *Appl. Catal., B* **2015**, *163*, 150−155.

(16) Lang, J.; Ma, Y.; Wu, X.; Jiang, Y.; Hu, Y. H. Highly Efficient Light-Driven Methane Coupling under Ambient Conditions Based on an Integrated Design of a Photocatalytic System. *Green Chem.* **2020**, *22*, 4669−4675.

(17) Jiang, W.; Low, J.; Mao, K.; Duan, D.; Chen, S.; Liu, W.; Pao, C.-W.; Ma, J.; Sang, S.; Shu, C.; Zhan, X.; Qi, Z.; Zhang, H.; Liu, Z.; Wu, X.; Long, R.; Song, L.; Xiong, Y. Pd-Modified ZnO−Au Enabling Alkoxy Intermediates Formation and Dehydrogenation for Photocatalytic Conversion of Methane to Ethylene. *J. Am. Chem. Soc.* **2021**, *143*, 269−278.

(18) Zhou, Y.; Zhang, L.; Wang, W. Direct Functionalization of Methane into Ethanol over Copper Modified Polymeric Carbon Nitride via Photocatalysis. *Nat. Commun.* **2019**, *10*, 506.

(19) Li, X.; Xie, J.; Rao, H.; Wang, C.; Tang, J. Platinum- and CuO$_x$-Decorated TiO$_2$ Photocatalyst for Oxidative Coupling of Methane to C$_2$ Hydrocarbons in a Flow Reactor. *Angew. Chem., Int. Ed.* **2020**, *59*, 19702−19707.

(20) Meng, L.; Chen, Z.; Ma, Z.; He, S.; Hou, Y.; Li, H. H.; Yuan, R.; Huang, X. H.; Wang, X.; Wang, X.; Long, J. Gold Plasmon-Induced Photocatalytic Dehydrogenative Coupling of Methane to Ethane on Polar Oxide Surfaces. *Energy Environ. Sci.* **2018**, *11*, 294−298.

(21) Wu, S.; Tan, X.; Lei, J.; Chen, H.; Wang, L.; Zhang, J. Ga-Doped and Pt-Loaded Porous TiO$_2$-SiO$_2$ for Photocatalytic Non-oxidative Coupling of Methane. *J. Am. Chem. Soc.* **2019**, *141*, 6592−6600.

(22) Yu, X.; Zholobenko, V. L.; Moldovan, S.; Hu, D.; Wu, D.; Ordomsky, V. V.; Khodakov, A. Y. Stoichiometric Methane Conversion to Ethane Using Photochemical Looping at Ambient Temperature. *Nat. Energy* **2020**, *5*, 511−519.

(23) Yu, X.; De Waele, V.; Löfberg, A.; Ordomsky, V.; Khodakov, A. Y. Selective Photocatalytic Conversion of Methane into Carbon Monoxide over Zinc-Heteropolyacid-Titania Nanocomposites. *Nat. Commun.* **2019**, *10*, 700.

(24) Song, H.; Meng, X.; Wang, S.; Zhou, W.; Wang, X.; Kako, T.; Ye, J. Direct and Selective Photocatalytic Oxidation of CH$_4$ to Oxygenates with O$_2$ on Cocatalysts/ZnO at Room Temperature in Water. *J. Am. Chem. Soc.* **2019**, *141*, 20507−20515.

(25) Song, S.; Song, H.; Li, L.; Wang, S.; Chu, W.; Peng, K.; Meng, X.; Wang, Q.; Deng, B.; Liu, Q.; Wang, Z.; Weng, Y.; Hu, H.; Lin, H.; Kako, T.; Ye, J. A selective Au-ZnO/TiO$_2$ hybrid photocatalyst for oxidative coupling of methane to ethane with dioxygen. *Nat. Catal.* **2021**, *4*, 1032−1042.

(26) Miao, T. J.; Wang, C.; Xiong, L.; Li, X.; Xie, J.; Tang, J. In Situ Investigation of Charge Performance in Anatase TiO$_2$ Powder for Methane Conversion by Vis-NIR Spectroscopy. *ACS Catal.* **2021**, *11*, 8226−8238.

(27) Yu, H.; Xu, L.; Wang, P.; Wang, X.; Yu, J. Enhanced Photoinduced Stability and Photocatalytic Activity of AgBr Photocatalyst by Surface Modification of Fe(III) Cocatalyst. *Appl. Catal., B* **2014**, *144*, 75−82.

(28) Shiozawa, T.; Kobayashi, T. High Resolution Electron Microscopic Study of Photolytic Silver in Silver Bromide. *Phys. Status Solidi* **1987**, *104*, 649−659.

(29) Zhang, H.; Wang, G.; Chen, D.; Lv, X.; Li, J. Tuning Photoelectrochemical Performances of Ag-TiO$_2$ Nanocomposites via Reduction/Oxidation of Ag. *Chem. Mater.* **2008**, *20*, 6543−6549.

(30) Zheng, Z.; Huang, B.; Qin, X.; Zhang, X.; Dai, Y.; Whangbo, M. H. Facile in Situ Synthesis of Visible-Light Plasmonic Photocatalysts M@TiO$_2$ (M = Au, Pt, Ag) and Evaluation of Their Photocatalytic Oxidation of Benzene to Phenol. *J. Mater. Chem.* **2011**, *21*, 9079−9087.

(31) Katsumata, H.; Hayashi, T.; Taniguchi, M.; Suzuki, T.; Kaneco, S. Highly Efficient Visible-Light Driven AgBr/Ag$_3$PO$_4$ Hybrid Photocatalysts with Enhanced Photocatalytic Activity. *Mater. Sci. Semicond. Process.* **2014**, *25*, 68−75.

(32) Wang, P.; Huang, B.; Qin, X.; Zhang, X.; Dai, Y.; Whangbo, M. H. Ag/AgBr/WO$_3$-H$_2$O: Visible-Light Photocatalyst for Bacteria Destruction. *Inorg. Chem.* **2009**, *48*, 10697−10702.

(33) Li, S.; Shen, Y.; Xie, A.; Yu, X.; Qiu, L.; Zhang, L.; Zhang, Q. Green Synthesis of Silver Nanoparticles Using Capsicum Annuum L. Extract. *Green Chem* **2007**, *9*, 852−885.

(34) Seyedmonir, S. R.; Strohmayer, D. E.; Geoffroy, G. L.; Vannice, M. A.; Young, H. W.; Linowski, J. W. Characterization of Supported Silver Catalysts. I. Adsorption of O$_2$, H$_2$, N$_2$O, and the H$_2$-Titration of Adsorbed Oxygen on Well-Dispersed Ag on TiO$_2$. *J. Catal.* **1984**, *87*, 424−436.

(35) Wang, Z.; Ma, W.; Chen, C.; Ji, H.; Zhao, J. Probing Paramagnetic Species in Titania-Based Heterogeneous Photocatalysis by Electron Spin Resonance (ESR) Spectroscopy-A Mini Review. *Chem. Eng. J.* **2011**, *170*, 353−362.

(36) Maheu, C.; Cardenas, L.; Puzenat, E.; Afanasiev, P.; Geantet, C. UPS and UV Spectroscopies Combined to Position the Energy Levels of TiO$_2$ Anatase and Rutile Nanopowders. *Phys. Chem. Chem. Phys.* **2018**, *20*, 25629−25637.

(37) Fu, C.; Li, F.; Yang, J.; Xie, J.; Zhang, Y.; Sun, X.; Zheng, X.; Liu, Y.; Zhu, J.; Tang, J.; Gong, X. Q.; Huang, W. Spontaneous Bulk-Surface Charge Separation of TiO$_2$-{001} Nanocrystals Leads to High Activity in Photocatalytic Methane Combustion. *ACS Catal.* **2022**, *12*, 6457−6463.

(38) Wood, P. M. The Potential Diagram for Oxygen at PH 7. *Biochem. J.* **1988**, *253*, 287−289.